Electric Power Systems Research 231 (2024) 110289

Contents lists available at ScienceDirect

Electric Power Systems Research

journal homepage: www.elsevier.com/locate/epsr

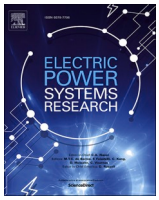

Emissions generated by electric vehicles in the 9-500 kHz band: Characterization, propagation, and interaction

Jon González-Ramos *, Alexander Gallarreta, Igor Fernández, Itziar Angulo, David de la Vega, Amaia Arrinda

University of the Basque Country (UPV/EHU), Bilbao, Spain

ARTICLE INFO

Keywords:
Conducted non-intentional emissions
Electric vehicles
Interaction
Low voltage grid
Propagation

ABSTRACT

Electric Vehicle Charging Processes (EVCPs), due to the involved power electronics with high-switching frequencies, generate high-amplitude emissions that could have a negative impact on Power Quality (PQ) and Narrowband Power Line Communications (NB-PLC) systems. In this context, this paper deals, first, with the frequency and time characterization of the disturbances generated by four EVCPs in the 9-500 kHz frequency range. The study is based on measurements carried out in a controlled Low Voltage (LV) grid. For this purpose, a novel procedure for the frequency and time characterization is proposed. The frequency characterization is based on the calculation of a set of parameters, which allows evaluating not only the amplitude of the disturbances in the frequency band under analysis, but also their spectral distribution. The time variability is characterized by means of a Fast Fourier Transform (FFT) analysis that leads to a simplified model to evaluate the time-dependent behavior of the disturbances, which shows a sub-cycle periodic pattern of the emissions in the frequency band of interest. Second, the propagation of the previously characterized emissions is analyzed, concluding that they propagate several meters through the LV grid. Although in most cases the disturbances are attenuated with distance, there might be resonances that lead to higher amplitudes at an electrical point distant from the source of the emissions. Finally, the influence of the simultaneous charging of several EVs is studied. The results show that, in general, the amplitudes correspond to the superposition of the individual disturbances, in addition to intermodulation products due to the switching frequencies of the inverters.

As a conclusion, the high amplitude time-varying emissions, together with their capacity for propagation and interaction, are a matter to be analyzed due to their influence on PQ and their potential degradation of the performance of PLC in the frequency band from 9 kHz to 500 kHz.

1. Introduction

Electric Vehicles (EVs) play a fundamental role in the concept of Smart Grid, and any Smart City initiative should include EV charging in their plans [1]. However, EVs face significant battery-related challenges, which lead to continuous innovation in order to improve aspects such as driving range, charging time, battery cost, etc. [2].

One unintended side effect of EV Charging Stations (EVCSs) is electromagnetic compatibility (EMC) issues due to conducted Non-Intentional Emissions (NIEs) [3], which may potentially impact Power Line Communications (PLC) [4–6]. Interfering emissions due to rectification caused by power electronics with high-switching frequencies up to several hundred kHz could propagate and have an effect not only close to the EVCS but also on the surrounding Low Voltage (LV) grid [7,8]. In order to cover all the frequency range where Narrowband PLC (NB-PLC) technologies can be developed, it is important to extend the

Abbreviations: CDF, Cumulative Distribution Function; EDF, Électricite de France; EMC, Electromagnetic Compatibility; EV, Electric Vehicle; EVCS, Electric Vehicle Charging Station; EVCP, Electric Vehicle Charging Process; FFT, Fast Fourier Transform; IFFT, Inverse Fast Fourier Transform; LISN, Line Impedance Stabilization Network; LV, Low Voltage; MV, Medium Voltage; NB-PLC, Narrowband Power Line Communications; NIEs, Non-Intentional Emissions; PFBL, Percentage of frequency bins exceeding the PLC out-of-band emission limits; PLC, Power Line Communications; POC, Point of Connection; PPS, Pulse per Second; PQ, Power Quality; QP, Quasi-Peak; SoC, State of charge; STFT, Short-term Fourier Transform; TSHV, Total Supraharmonic Voltage.

* Corresponding author.

E-mail addresses: jon.gonzalezr@ehu.eus (J. González-Ramos), alexander.gallarreta@ehu.eus (A. Gallarreta), igor.fernandez@ehu.eus (I. Fernández), itziar.angulo@ehu.eus (I. Angulo), david.delavega@ehu.eus (D. de la Vega), amaia.arrinda@ehu.eus (A. Arrinda).

https://doi.org/10.1016/j.epsr.2024.110289
Received 8 June 2023; Received in revised form 11 October 2023; Accepted 27 February 2024
Available online 16 March 2024

study of these emissions from the classical supraharmonic range (2–150 kHz) [9] to the frequency band up to 500 kHz. In this context, this paper is focused on the characterization of the NIEs generated by Electric Vehicle Charging Processes (EVCPs) in a controlled LV grid in the frequency range 9-500 kHz, in addition to analyzing their capacity of propagation and interaction. The study is based on measurements carried out in a controlled LV grid scenario.

2. State of the art

2.1. Non-Intentional emissions generated by EVCPs

The effect of the penetration of EVs on the Power Quality (PQ) parameters (up to 2 kHz) has been deeply studied in the existing literature [10–12]. Although according to [13], the rectifiers included in the circuitry for the battery charging process are a source of high-amplitude emissions, only a few research works have been carried out for their proper characterization in the supraharmonic range (2 kHz to 150 kHz).

In [14], the main causes of the spectral components of the emissions generated by an electric bus in the 2-150 kHz frequency range are identified. In [7], the supraharmonic currents of a bidirectional EVCS are measured and analyzed in the frequency domain, showing both wide-band and narrow-band emissions. Similarly, reference [15] analyzes the supraharmonic emissions generated by nine popular EV models in the Netherlands for frequencies up to 100 kHz. As stated in [16] and [17], the spectral pattern of the disturbances is highly dependent on the EV model and the charging regime, and thus, extensive measurement campaigns are necessary to model this type of NIEs.

The authors of the current work also presented a time- and frequency-characterization of the conducted disturbances generated by two commercial EV models from 9 kHz up to 500 kHz in [18]. The measurements analyzed in [18] were performed on an artificial Line Impedance Stabilization Network (LISN). However, conducted emissions in real scenarios will strongly depend on local grid conditions and the influence and interaction with other electrical equipment connected close-by [7].

Therefore, the current state-of-the-art presents some research gaps that still need to be covered in this area. First, there are scarce studies available for the frequency range above 150 kHz, so that their potential negative effect on NB-PLC technology covering the frequency band up to 500 kHz is unknown. Second, as already shown in the literature, the conducted emissions depend on the specific charging process (EVCS, EV model and state of charge). This highlights the need for extensive measurement campaigns considering different charging situations, in order to provide a big picture of the current and future situations of EV development.

2.2. Propagation and interaction of NIEs

The conducted disturbances in this frequency range have been proven to propagate over several kilometers in the LV and Medium Voltage (MV) grids [19–21]. Moreover, as in a real situation an EV is surrounded by other sources of disturbances, the resultant emissions at a certain electrical point are expected to be the combination of the propagated emissions generated by each source. For this reason, in order to fully determine the effects of the EVCPs on the amplitude of the emissions in the LV grid, it is essential not only to properly characterize these emissions in the time and frequency domains at the Point of Connection (POC) where the EVCS is installed, but also to analyze their propagation and interaction with other connected equipment.

Up to now, several laboratory and on-site measurements have been carried out for the characterization of the interaction of the disturbances generated by different electronic devices. According to the existing studies, the disturbances measured at the terminal of a certain device consist of a primary and a secondary emission. The primary emission, dependent on the grid impedance and, therefore, on the location and time of the day, is defined as the part of the current generated by the sources inside the device. In contrast, the secondary emission corresponds to the part of the current originated by sources outside the device [19,22–27]. In [24], where a model for estimating the emissions of a laboratory installation composed of multiple devices is presented, it is stated that this secondary emission cannot be disregarded and should be taken into account for the correct characterization of the resultant emission generated by an individual appliance.

In [23], by means of a simulation model, the influence of the length of the line on the disturbance levels is studied. For that purpose, the interaction between some specific devices connected at the same and different electrical points has been considered. The study in [23] is based on the analysis of the emissions at specific frequencies depending on the number of connected devices and the length of the electrical cable.

Some works have also analyzed the influence of the interaction between electronic equipment in a laboratory environment. This interaction depends on the devices and the characteristics of the source impedance [19], and the time of the day [28]. According to the authors of those contributions, the emissions generated from a specific device increase if more appliances are connected at the same electrical installation, whereas the total emission of the grid is reduced [24].

Regarding the propagation and interaction of the emissions generated by EVCPs, in [29], the long-term variations of the NIEs generated from three electric charging infrastructures are analyzed up to 100 kHz, both in the frequency and time domains. The conclusion of the work is that the higher the number of EVs, the higher the disturbances measured in the power grid. A similar study is performed in [30], where the time and frequency analysis of the behavior of the supraharmonics from EVCSs is addressed for frequencies up to 100 kHz in laboratory conditions.

However, the existing literature only considers the propagation of emissions from individual devices, without analyzing the cumulative effect of NIEs from several sources on their propagation through the grid. Moreover, as stated in [31], the disturbances generated by electronic appliances show a considerable time-dependent behavior and, consequently, the propagation analysis can only be carried out by means of synchronized measurements at different electrical points [32].

Consequently, the state-of-the-art shows that the aggregation of simultaneous emissions from various EV charging processes should be investigated. Finally, conducted NIEs from EVs should be analyzed in more realistic grid conditions, avoiding uncontrolled grid factors, in order to evaluate propagation and interaction with other electrical equipment.

3. Paper contributions and structure

Considering the research gaps presented above, the main objective of this paper relies on the frequency and time characterization of the emissions generated by a set of EVs during their charging process in the 9-500 kHz frequency range. The study, based on measurements carried out in a controlled LV grid, proposes a novel procedure that allows evaluating a certain disturbance by means of the calculation of a set of parameters and a Fast Fourier Transform (FFT) analysis. Moreover, the propagation of the NIEs along the grid is analyzed by means of synchronized measurements at different connection points. Finally, in order to study the interaction of the emissions from various EVCPs, the aggregation of simultaneous emissions is investigated.

With the aim of highlighting the novelty of this paper, Table I shows a summary of the previously presented state of the art, in addition to the main contributions of the current paper.

The rest of the paper is organized as follows. In section IV, the measurement scenario is presented, including the available technical specifications of the EVCSs under study, as well as the measurement system used for the recording of the NIEs and the signal processing. In section V, the NIEs generated by four different EVCPs are characterized

Table I
Summary of the previously presented state of the art and the main contributions of the current paper.

Reference	Frequency range	Measurement scenario	Scope of the study
Grasel, [7]	9-150 kHz	Reconstructed LV grid	Characterization of the conducted emissions generated by a V2G EVCS
Meyer, [13]	50 Hz-150 kHz	Laboratory	Characterization of the conducted emissions generated by 19 EVCPs
Lodetti, [14]	2-150 kHz	Point of Common Connection (LV grid)	Characterization of the conducted emissions generated by an electric bus inductive charging
Slangen, [15]	0-100 kHz	Testlab of ElaadNL	Characterization of the conducted emissions generated by 9 EVCPs
Schöttke, [16]	2-150 kHz	Laboratory/LV grid	Characterization of the conducted emissions generated by 6 EVCPs
Darmawardana, [17]	2-150 kHz	LV grid/Waveform generator (supply)	Characterization of the conducted emissions generated by two EVCPs
González-Ramos, [18]	9-500 kHz	LISN	Characterization of the conducted emissions generated by two EVCPs
Espín-Delgado, [20]	2-150 kHz	LV grid (TU Dresden laboratory)	Propagation and interaction study of the conducted emissions generated by PV inverters and LEDs based on a correlation and impedance analysis
Cassano, [23]	5.1 kHz and 15.1 kHz	Simulations (LV grid)	Propagation and interaction analysis of the conducted emissions generated by a fast DC EVCS based on a primary/secondary emission approach
Sutaria, [26]	2-150 kHz	Laboratory at the University of Luleå	Characterization of the conducted emissions generated by different Power Factor Corrected circuits. The propagation of these emissions is analyzed based on a primary/secondary emission approach
Streubel, [29]	2-150 kHz	Three different parking garages with charging infrastructures	Characterization of the conducted emissions generated by three EV charging infrastructures in the long-term
Slangen, [30]	0-100 kHz	Smart Grid Interoperability Lab	Characterization of the conducted emissions generated by four EVs. The propagation and interaction of these emissions are analyzed based on a primary/secondary emission approach
Current paper	9-500 kHz	Controlled LV distribution grid	Definition of a novel procedure for the characterization of the conducted emissions generated by four EVCPs (time and frequency domains). The propagation and interaction of these emissions is analyzed based on synchronized measurements at different electrical points in the LV distribution grid

in the frequency and time domains up to 500 kHz. In section V.A, the Quasi-Peak (QP) values of the amplitude of the disturbances, according to the CISPR16-1-1 [33], are presented. The study of the time-variant behavior of the disturbances over the measurement time is discussed in section III.B. In sections VI and VII, the propagation and interaction of the emissions previously characterized are addressed. Finally, in section VIII, the main conclusions of the work are gathered.

4. Methodology

4.1. Description of the measurement scenario

The measurements that support this study are carried out in the "Concept Grid" laboratory of Électricite de France (EDF), a unique testing facility that goes beyond ideal conditions of laboratory trials, but at the same time, avoids uncontrolled background distortion that may substantially affect the results [7]. This testing scenario simulates a LV distribution grid composed of a Secondary Substation (SS) and five houses, with a three-phase installation, to which different electronic devices can be connected.

In this study, three different EVCSs are analyzed. EVCS1 is installed at H2, EVCS2 at H3, and EVCS3 at H5. There are 3 EV models available, and each EV model can only be charged at its corresponding EVCS. A representation of the measurement scenario is shown in Fig. 1, where the distance between the different houses and the location of the EVCSs are indicated.

In order to have a predominantly resistive load at the POC, domestic heaters were connected to each house. The background noise due to these loads was characterized at H4, considering this as the default situation. All the measurement results presented in the following sections were conducted in the same electrical phase (monophasic measurements).

The four situations to be analyzed correspond to the charging process of EV1 at 81% state of charge (SoC), EV2 at 100% and 75% SoC, and EV3 at 68% SoC. The disturbances were measured at the POC of each house to which the EVCS under study is installed. As the emissions generated by EVCP1 and EVCP3 were only measured at a given SoC, hereafter the SoC of these two EVCPs will not be specified each time these two EVCPs are cited in the text. In order to analyze the propagation of the emissions generated by each EVCP individually, synchronized measurements were carried out at H2, H3, and H5. The analysis of the interaction of the NIEs is based on measurements performed at H2, H3, and H5 when the three EVs are charging simultaneously.

Limited technical information of the EVCSs under study is available, with no information about EVCS2. In Table II, the technical specifications of EVCS1 and EVCS3 are gathered. In all the trials, EVCS1 corresponds to the charging post of EV1, EVCS2 to the charging circuitry of EV2, which is installed inside EV2, and EVCS3 to the charging post of EV3.

4.2. Measurement system for NIEs

The measurement system for NIEs, shown in Fig. 2, is based on the voltage probe presented in [36], which is connected to the electrical point where the disturbances are measured. This voltage probe shows a flat response for a wide range of impedance values that may be found in the grid. A digital oscilloscope, controlled by a laptop, is responsible for recording the signal with high accuracy (15 bits of resolution in magnitude) and a high sampling frequency (8.92 MHz). The acquisition of the NIEs is performed by means of purpose-specific software developed by the authors.

In order to carry out synchronized measurements at three different

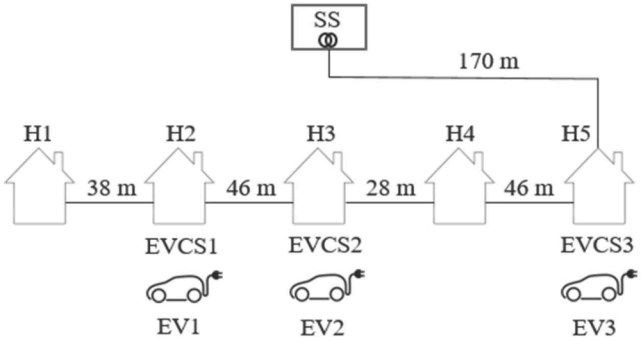

Fig. 1. Measurement scenario in the "Concept Grid" laboratory of EDF in Écuelles.

Table II
Technical specifications of EVCS1 and EVCS3 [34,35].

EVCS	Model	Mode	Output Voltage	Output Current	Maximum single-phase power
EVCS1	NSQC442G	3	50–500 V DC	0 – 120 A DC	–
EVCS3	Witty-XEV100	3	230-400 V (Adjust.)	–	32 KVA

locations, three measurement systems as the one presented in Fig. 2 are needed, as well as an identical time setting in each computer. For this purpose, a GPS module is required for generating a Pulse per Second (PPS) signal with a precision of 20 ns. In this way, a deviation between computers of less than a millisecond is achieved. In each measurement, the GPS signal is recorded at the same time as the disturbances.

4.3. Signal processing

Once the emissions are recorded, the results are represented in a color scale with respect to frequency (horizontal axis) and time (vertical axis) in the form of spectrograms by means of a Matlab script, providing a time and frequency resolution of 2 ms and 50 Hz, respectively. For this purpose, a sliding Lanczos windowing with a duration of 20 ms and an overlapping of 90% between consecutive windows is applied. The Lanczos window is defined in (1),

$$w[n] = \begin{cases} sinc\left(2\left(\frac{2n}{N-1}\right)\right) sinc\left(\frac{2n}{N-1}-1\right), & n \neq \frac{N-1}{2} \\ 1, & n = \frac{N-1}{2} \end{cases}, \; n = 0, 1, \ldots, N-1 \tag{1}$$

where N is the number of samples per 20 ms window.

Then, in order to obtain the measured spectrum every 2 ms, a Short-Term Fourier Transform (STFT) is applied to each time window according to (2),

$$Z[f_c, k] = \sum_{n=0}^{N-1} x[n-k]w[n]e^{-j2\pi fn} \tag{2}$$

where f_c are the frequency components, and k the time steps between consecutive STFT outputs.

As the recordings of the emissions last 600 s (except for EV2 at 75% SoC, where the emissions were recorded for 250 s), due to computational effort, only 50 s of the recordings are represented. As an example, Fig. 3 shows the spectrogram during the first 50 s of the emissions generated by the charging process of EV1.

Subsequently, in order to characterize the disturbances in the frequency domain, the QP values of the amplitude of the emissions are obtained according to CISPR 16–1-1 standard [33], obtaining a single figure of QP values of the amplitude of the NIEs as a function of frequency for each time interval of 50 s.

By contrast, the time characterization of the emissions is performed by evaluating the variability of each frequency bin over the measurement time.

5. Characterization of individual emissions

5.1. Frequency analysis

Fig. 4 shows the QP values of the amplitude of the emissions generated by the EVCP1, EVCP2 at 75% and 100% SoC, and EVCP3, respectively, together with the emissions corresponding to the default situation.

As no emission limits have been specified for the conducted disturbances generated by EVs during the charging process, the out-of-band limits defined for communications equipment in EN 50065-1 [37] might be considered as a conservative criterion [38] for comparison purposes.

In general, the amplitude of the emissions is very high if compared to the background noise corresponding to the default situation in which no EV is connected to the grid. This does not go in line with the observations in [16], where no significant emission is visible above 50 kHz. This reinforces the idea that the emissions are very dependent on the specific characteristics of the charging process under analysis.

For EVCP1 and EVCP2, the measured disturbances are in the form of harmonics of the switching frequency of an inverter of the EV charger [7],[13],[16]. For instance, Fig. 4(a) shows this spectral pattern, where harmonics of 10 kHz (amplitudes between 62 dBμV and 98 dBμV) are measured in the whole frequency band. In the case of EVCP2, harmonics of 16 kHz with amplitudes varying between 82 dBμV and 115 dBμV at 75% SoC and between 82 dBμV and 106 dBμV at 100% SoC are registered. By contrast, as shown in Fig. 4(c), a high-amplitude emission decreasing with frequency in the form of colored noise is observed for EVCP3 between 70 kHz and 500 kHz (amplitudes varying from 79 dBμV

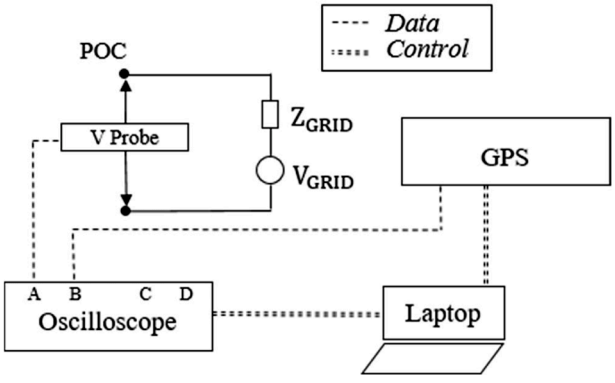

Fig. 2. Measurement system for Non-Intentional Emissions.

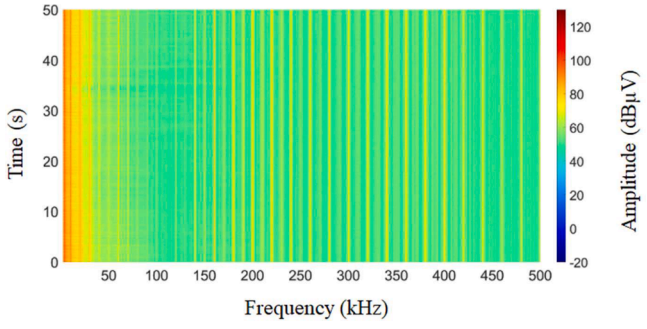

Fig. 3. Spectrogram of the disturbances generated by the charging process of EV1 during 50 s.

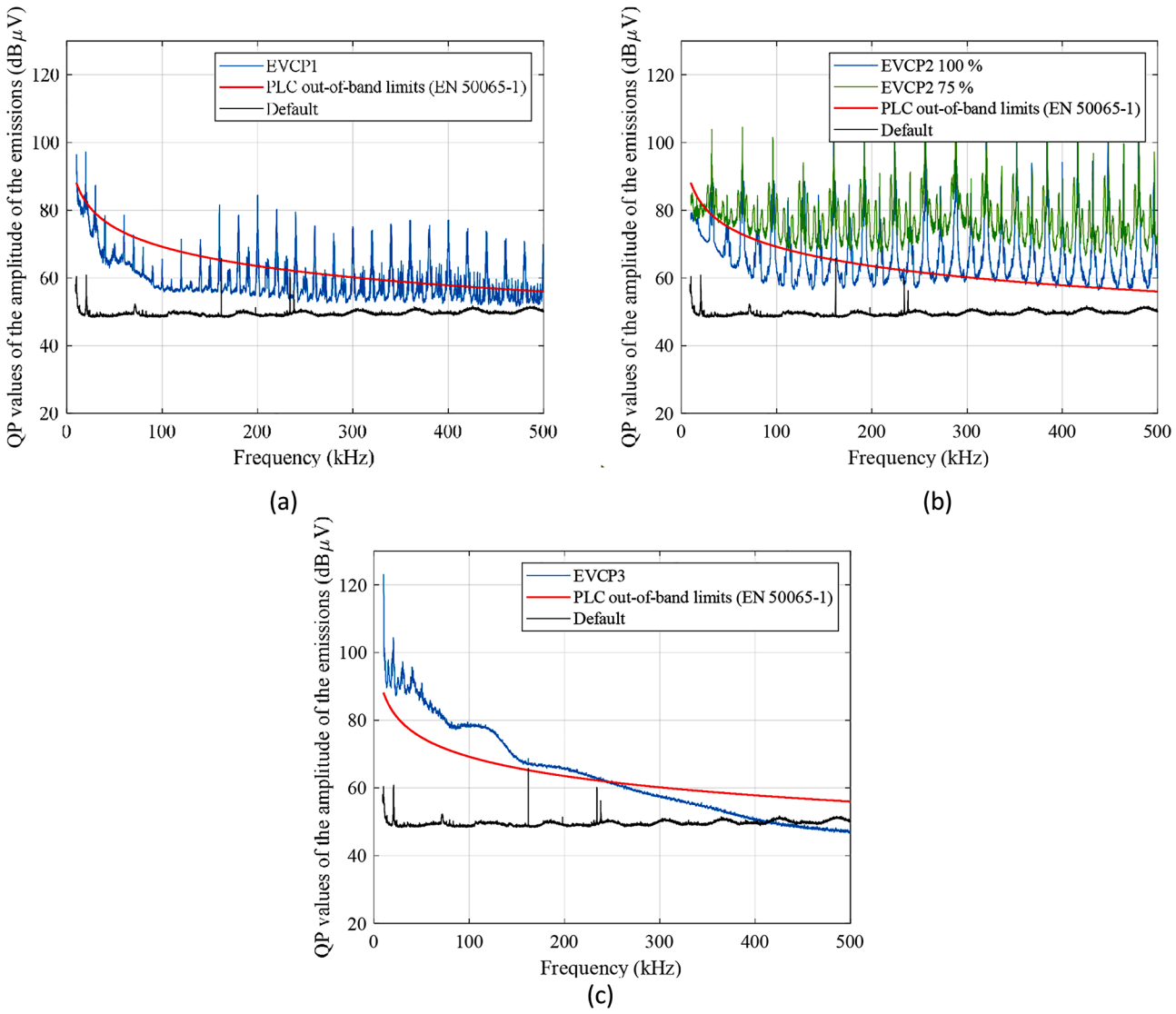

Fig. 4. QP values of the amplitude of the emissions (dBμV) generated by EVCP1 (a), EVCP2 at 75% and 100% SoC (b), and EVCP3 (c).

to 48 dBμV). This might be due to an efficient grid-side filter circuit, PWM-controlled devices using active power factor correction and/or a control regime that continuously changes the switching frequency [7,13, 30]. In order to verify this, a time domain analysis is required (see section V.B).

Moreover, Fig. 4(b) demonstrates that the amplitudes of the spectral components do not necessarily decrease with frequency, as observed in [14]. Fig. 4(b) also shows that the spectral pattern varies with the state of charge [13,16,39]. Although similar amplitudes are obtained at the narrowband emissions if both states of charge are compared, there is a minor shift in the fundamental frequency of the spectral components and, hence, the high-amplitude narrowband emissions are not centered at exactly the same frequencies. This effect is also found in the results presented in [13,17]. As an example, Fig. 5 shows the emission generated by the charging process of EV2 at 100% and 75% SoC around 350 kHz. The peaks of the emission are located at 351.9 kHz and 352.4 kHz respectively.

Therefore, the previous figures clearly show that the QP values of the amplitude of the emissions highly depend on the particularities of the EVCPs (EVCS, EV model and state of charge), as different spectral components and amplitudes of the emissions have been registered. This effect might be caused by the filter circuits of the EVs [13]. Considering that the details of the electronic components are not usually provided by the manufacturers, this highlights the need for basing the analysis of emissions from EVCPs on experimental evidence [17].

In order to numerically characterize the QP values of the amplitude of the emissions for the whole frequency band of interest, the Total Supraharmonic Voltage (TSHV) [40–42] is calculated for the four situations under study according to (3).

$$\mathrm{TSHV} = \sqrt{\sum_{i=1}^{i=9821} \mathrm{V_i}^2} \tag{3}$$

This parameter, calculated in linear scale and then converted to logarithmic, gives a general overview of the amplitude of the disturbances generated by each EVCP in the whole frequency band. The summation considers the QP values of the amplitude of the emissions of the 9821 frequency bins covering the band under analysis (9-500 kHz) with a frequency step size of 50 Hz.

Moreover, in order to determine if the emissions above the limit are concentrated at specific frequencies or spread over wider frequency bands, the percentage of frequency bins exceeding the PLC out-of-band emission limits (PFBL) is calculated.

$$\mathrm{PFBL} = \frac{\text{number of frequency bins above the limit}}{\text{total number of frequency bins}} \cdot 100 \tag{4}$$

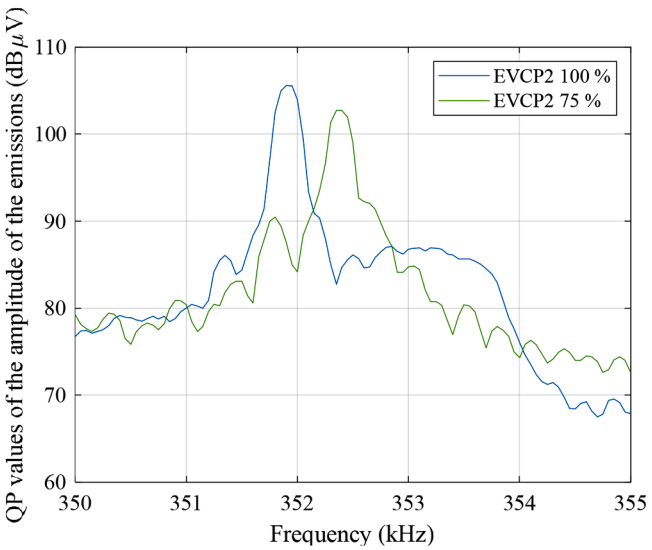

Fig. 5. Frequency shift of the emission generated by EVCP2 around 350 kHz for different states of charge.

In Table III, the TSHV and PFBL are gathered for each situation under study.

Table III clearly shows that the emissions generated by the charging process of EV1 in the 9-500 kHz frequency band are considerably lower in comparison with EVCP2 and EVCP3 (differences between 9 dB and 19 dB), in addition to being concentrated in fewer frequency bins (18%). If the TSHV values for EVCP2 at 75% and 100% SoC are compared, it can be concluded that the emissions introduced by this EVCP are higher when EV2 is not fully charged. This difference in the emission amplitudes is also reflected in the noise floor obtained at 75% and 100% SoC, which explains the change in the PFBL from 97% at 75% SoC to 62% at 100% SoC. Finally, it should be mentioned that, despite distributing the emissions in only 48% of the frequency bins, the charging process of EV3 generates the highest disturbance amplitudes according to the TSHV.

The PFBL shows if the emission amplitudes above the PLC out-of-band emission limits are concentrated at particular frequencies or spread over wider frequency bands, but it does not reflect the spectral distribution of the emissions over the 9-500 kHz frequency band. In order to show the spectral distribution of the emissions above the PLC out-of-band emissions limits, the Cumulative Distribution Function (CDF) of the frequency bins that correspond to emission amplitudes above the emission limit is calculated for each situation under test. In Fig. 6, the obtained CDFs for EVCP1, EVCP2 at 75% and 100% SoC, and EVCP3, are depicted.

As shown in Fig. 6, the slope of the CDF of EVCP1 is much steeper at frequencies above 150 kHz, which implies that a higher number of frequency bins exceed the PLC out-of-band emission limits in the frequency range 150-500 kHz. A similar behavior is observed above 70 kHz if the CDF of EVCP2 at 100% SoC is analyzed. Regarding the CDF obtained for EVCP2 at 75% SoC, a linear trend is shown in almost the whole frequency band of analysis, which demonstrates a continuous uniform distribution from 23 kHz to 500 kHz (i.e., all the emissions are above the limit in this frequency range). Again, the difference in the results obtained for both SoCs is affected by the difference in the noise

Table III
TSHV and PFBL for each EVCP.

EVCP	TSHV	PFBL
EVCP1	112 dBμV	18%
EVCP2 75%	128 dBμV	97%
EVCP2 100%	121 dBμV	62%
EVCP3	131 dBμV	48%

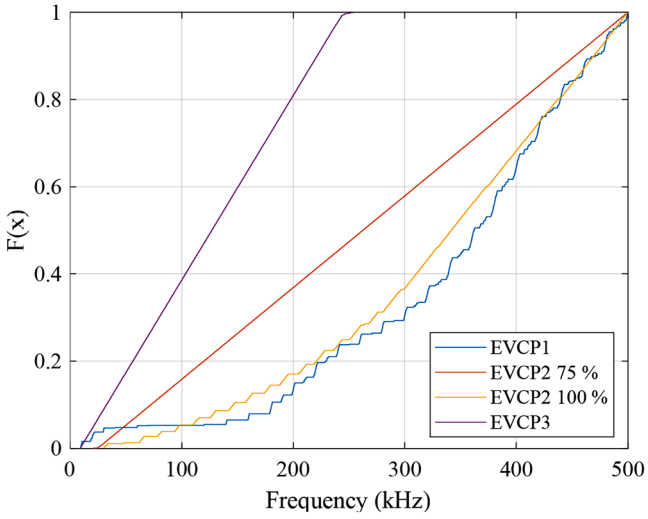

Fig. 6. CDFs of the frequency bins that correspond to QP emission amplitudes above the PLC out-of-band emission limits.

floor measured in the two situations. Finally, the CDF of EVCP3 allows to conclude that, as shown in Fig. 6, all the frequency bins exceed the limits between 9 kHz and 250 kHz (uniform distribution in this frequency band).

These results are of practical interest for planning PLC systems in this frequency band because, as shown in Fig. 4, the QP values of the amplitude of the emissions generated in the four situations under study exceed the limits defined for the PLC out-of-band emissions at least for some frequency bands. If the eight channels defined for PRIME v1.4 are considered [43], and evaluating the CDFs obtained in Fig. 6, it is possible to opt for the communication channels that present lower disturbance amplitudes. For example, in presence of emissions similar to the situation corresponding to the charging process of EV1, channel 1 (42-89 kHz) and channel 2 (97–144 kHz) would present better channel conditions in terms of disturbances, as very few spectral components of the emissions are above the PLC out-of-band emission limits. In the case of EV3, channels 5 (261-308 kHz), 6 (315–362 kHz), 7 (370–417 kHz) and 8 (424-471 kHz) would imply less disturbances caused by the EVCP.

5.2. Time analysis

The measurements give rise to spectrograms that are composed of many samples corresponding to each frequency bin and time instant, which cover a wide range of amplitude values. Therefore, due to computational issues, the analysis in the time domain is performed for shorter time periods of 50 s length.

The analysis of the time variability of the disturbances is organized as follows. First, in section V.B.1), the differences in the QP values of the amplitudes of the emissions are compared for the resultant time periods of 50 s. Second, in V.B.2), the variations over time given within the first 50 s period of each recording are modelled by means of a FFT analysis.

5.2.1. Analysis of the time variability within the recording time

The analysis of the time variability within the recording time is based, first, on the comparison of the QP values of the amplitude of the emissions calculated over each period of 50 s within that recording time (600 s, i.e. 12 periods, except for EVCP2 at 75% SoC, where 250 s are available, i.e. 5 periods). In Fig. 7, the QP values of the amplitude of the emissions generated by the charging process of each EV over each period of 50 s are superimposed, together with the PLC out-of-band emissions limits.

Although the spectral form of the emissions is maintained in the whole frequency band for the consecutive periods of 50 s for the four

situations under study, slight variations in the amplitude of the disturbances can be observed at certain frequencies. For this reason, in order to quantify these differences, the TSHV and PFBL are calculated for the 12 periods of 50 s (5 periods in the case of EVCP2 at 75% SoC). Then, the following figures are obtained in order to characterize the maximum difference of the TSHV (ΔTSHV) and PFBL (ΔPFBL) for each analyzed situation:

$$\Delta\text{TSHV} = \max_{i\in\{1,2,\ldots n\}} \text{TSHV}_i - \min_{i\in\{1,2,\ldots n\}} \text{TSHV}_i \quad (5)$$

$$\Delta\text{PFBL} = \max_{i\in\{1,2,\ldots n\}} \text{PFBL}_i - \min_{i\in\{1,2,\ldots n\}} \text{PFBL}_i \quad (6)$$

where $n = 12$ except for EVCP2 at 75% SoC, where $n = 5$. In Table IV, ΔTSHV and ΔPFBL values for each EVCP are gathered.

In the case of EVCP1, a maximum difference of the TSHV of 3 dB is observed between different periods of the emissions generated by its charging process. In the remaining analyzed cases, these differences do not exceed 1 dB. Regarding the PFBL, in the cases of EV1 and EV2 at 75% SoC, maximum differences of 1% and less than 1% are obtained, respectively. The differences in the PFBL for EV2 at 100% SoC and EV3, in turn, increase up to 11% and 6%, respectively. However, these larger differences do not result in great variations in the TSHV in that cases, which implies that the emissions exceeding occasionally the limits do not present high amplitude. Therefore, it can be concluded that, in general, the disturbances generated by the EVCPs under study present a quasi-stationary behavior in periods ranging from 50 s to several minutes.

Table IV
ΔTSHV and ΔPFBL.

	ΔTSHV	ΔPFBL
EVCP1	3 dB	1%
EVCP2 at 75% SoC	1 dB	0%
EVCP2 at 100% SoC	0 dB	11%
EVCP3	1 dB	6%

Apart from that, although not explicitly shown in Table III, it is important to highlight that the TSHV of the last period of 50 s for EV2 at 75% SoC (129 dBμV) is significantly higher if compared to the TSHV recorded for the first 50-second period at 100% SoC (122 dBμV). This means that the emissions can substantially differ for different states of charge. Therefore, despite the fact that it is not possible to determine when these time variations occur, it can be assumed that variations

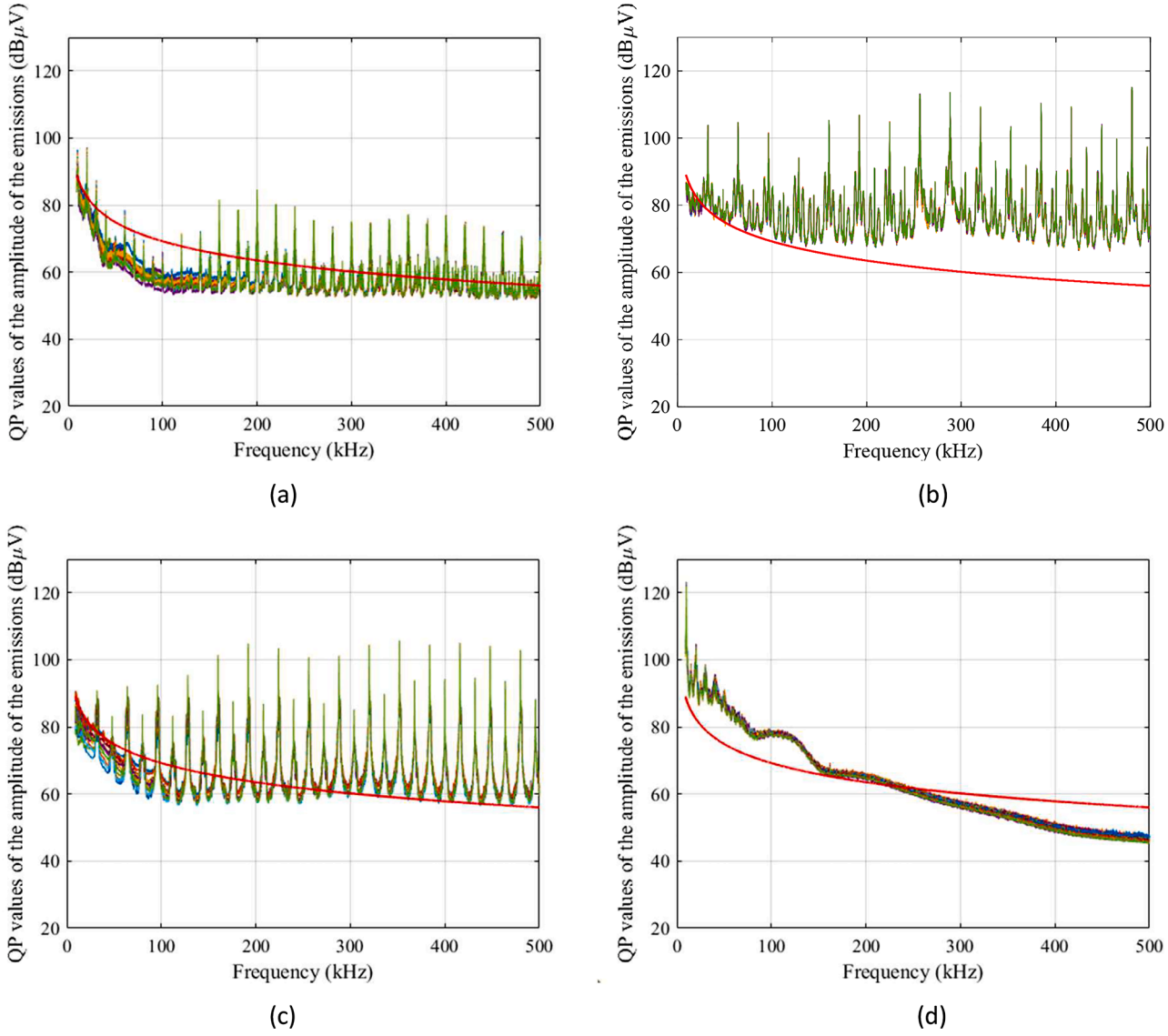

Fig. 7. QP values of the amplitude of the emissions (dBμV) generated by EVCP1 (a), EVCP2 at 75% (b) and 100% (c) SoC, and EVCP3 (d) in each period of 50 s within the recording time.

given in periods greater than several minutes due to changes in the state of charge are to be expected. As EVs use constant current/constant voltage modes for charging their batteries [44], this effect can be due to the charging profile of these two modes. Abrupt differences in the emission amplitudes 30 minutes after start of the charging cycle have been also reported in [16].

5.2.2. Analysis of the time variability within 50 s

In the previous section, it was concluded that no time variations in periods longer than 50 s are occurring, since similar TSHV and PFBL were obtained in each 50-second period within the recording time. For this reason, time variations can only occur in periods of less than 50 s. In order to quantify this potential time variability, a FFT is applied to the time samples corresponding to the first 50-second period of each frequency bin of the spectrogram, obtaining the FFT frequency components of the time variability of each frequency bin.

With the aim of comparing the amplitudes of the FFT frequency components corresponding to the different frequency bins, the resultant FFTs are normalized with respect to the corresponding amplitude of the FFT component at 0 Hz. As an example, in Fig. 8, the modulus of the normalized FFT obtained for the first 50-second period of the emissions generated by the charging process of EV2 at 100% SoC at the frequency bin 383.901 kHz is presented. Fig. 8 only shows the positive part of the FFT spectrum, since the emissions generated by the charging process of an EV are real signals, whose FFT is even.

In the 39,284 analyzed frequency bins (9821 frequency bins/signal · 4 signals), the modulus of the normalized FFTs were similar to the one shown in Fig. 8, where narrowband FFT components at 50 Hz, 100 Hz, 150 Hz, 200 Hz and 250 Hz are observed. This FFT pattern corresponds to a periodic function with period T = 1/50 = 20 ms [45].

Therefore, the normalized FFT, regardless of the frequency bin and EVCP under study, can be characterized by a simplified model composed of the main components at 50 Hz, 100 Hz, 150 Hz, 200 Hz, and 250 Hz. For each frequency bin, the main amplitude of those components is detected using the normalized FFT in dB, as represented in Fig. 8. Then, a simplified model is proposed in linear scale according to (7):

$$\mathrm{FFT}\ (\mathrm{f_{FFT}}) = \delta(\mathrm{f_{FFT}}) + \sum_{n=1}^{5} \mathrm{c_n}\cdot\delta(\mathrm{f_{FFT}} - 50\mathrm{n}) \tag{7}$$

where $\delta(\mathrm{f_{FFT}})$ is the unit sample function.

In (7), $\mathrm{c_n}$ are 2π times the complex Fourier coefficients of the signal, given in linear scale and normalized with respect to the 0 Hz FFT component.

With the aim of determining how the original signal resembles the signal obtained by approximating the FFT with the proposed simplified model (synthesized signal), the absolute value of the Inverse FFT (IFFT) of the impulse train in (7) is calculated and expressed in logarithmic scale. For this purpose, the non-normalized coefficients in (7) are considered. In Fig. 9, the original and synthesized emissions generated by the charging processes of EVCP2 at 100% SoC at 255.951 kHz (a) and EVCP3 at 10 kHz (b) are shown during a time period of 0.11 s.

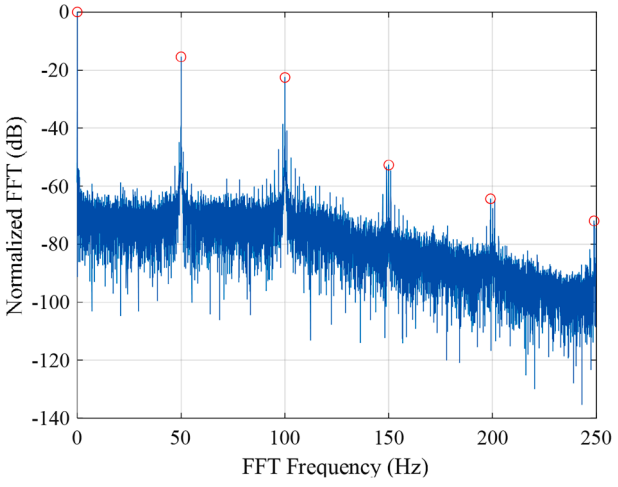

Fig. 8. Modulus of the normalized FFT (dB) of the time samples corresponding to the emissions generated by EVCP2 at 100% SoC at 383.901 kHz.

As it can be observed, the synthesized signal approximates accurately the amplitude of the original signal, as well as the peak-to-peak and the shape of the variation. This means that the complex coefficients of the simplified model $c_n$provide a quantitative characterization of the signal variation in the time domain. Therefore, in order to quantify the total time variations of the emissions and relate their time-dependent behavior with their spectral characteristics, the total variability of the disturbances is calculated, as shown in (8), as the sum in linear scale of the modulus of the amplitude of the FFT components at 50 Hz, 100 Hz, 150 Hz, and 200 Hz, which is then converted to logarithmic.

$$\text{Total variability (dB)} = 20\cdot\log_{10}\left(\sum_{n=1}^{4}|\mathrm{c_n}|\right) \tag{8}$$

For the two examples shown in Fig. 9, the total variability is -11.8 dB for (a) and -7.9 dB for (b), so that the higher the sum of the FFT components, the greater the variation of the signal over time.

Fig. 10 shows the total variability of the disturbances obtained in terms of the FFT components, along with the QP values of the amplitude of the emissions.

Similarly as obtained for the frequency analysis, the time variations of the amplitudes of the NIEs also depend on the specific charging process (EVCS, EV model, and state of charge). Finally, from Fig. 10 it can be assumed that, while the background noise remains practically static over time in the four charging situations under study, higher variations occur at the frequency bins corresponding to disturbances, both for narrowband emissions and colored noise.

6. Propagation of the measured emissions

6.1. Frequency analysis of the propagation of the emissions

In order to analyze the propagation of the emissions in the frequency domain, the QP values of the amplitude of the emissions measured at H2, H3, and H5 are superimposed when each EV model is charged individually. Fig. 11 shows, for the three measurement locations, the emissions generated by the charging process of EV1 (a), EV2 at 75% (b) and 100% (c) SoC, and EV3 (d).

As it can be seen, the emissions do not remain in the proximity of the source and they propagate several meters through the electrical grid. In most of the cases, the spectral patterns of the disturbances are maintained, but they are attenuated with the distance. In order to clearly observe this behavior, Fig. 12 shows, as an example, a zoom of the QP values of the amplitude of the emissions (dBμV) generated by EVCP1 measured at H2, H3, and H5 in the frequency range 230-250 kHz.

If the emission at 240 kHz is taken into account, a decrease in the amplitudes generated by the charging process of this EV model can be observed when measuring at distances of 46 m (POC of H3) and 120 m (POC of H5). The generated emission suffers an attenuation of 5 dB (from 79.5 dBμV to 74.5 dBμV) if the NIEs are measured at H3, while the attenuation increases up to 10.7 dB (from 79.5 dBμV to 68.8 dBμV) at H5.

By contrast, at certain frequencies of the spectrum when EV1 is charging, higher emissions are measured at locations different to the POC of the source. As an example, Fig. 13 presents the QP values of the amplitude of the emissions generated by EVCP1 at H2, H3, and H5 in the frequency range 70-90 kHz. Despite EV1 being charged at H2, the component around 80 kHz is greater when measured at H5 than when measured at the same POC where the EV is charging.

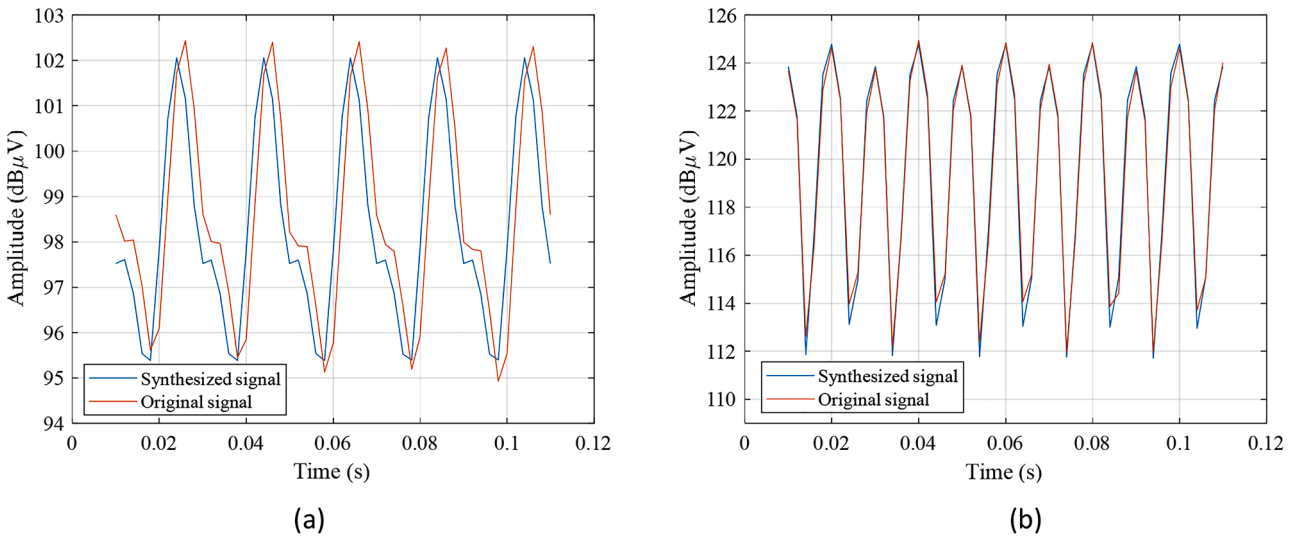

Fig. 9. Synthesized and original emissions generated by the charging processes of EVCP2 at 100% SoC at 255.951 kHz (a) and EVCP3 at 10 kHz (b).

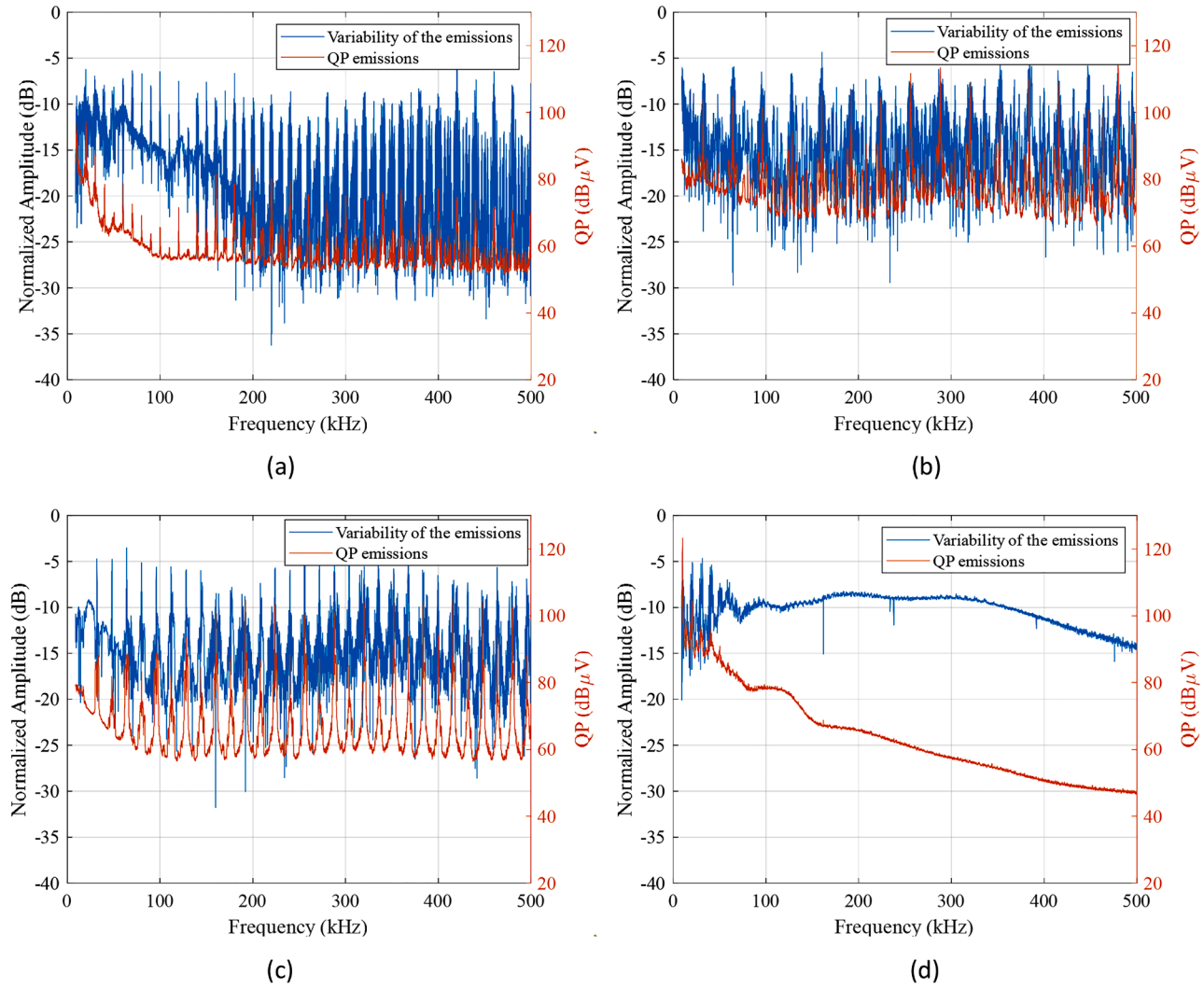

Fig. 10. Normalized amplitude (dB) of the variability of the emissions generated by EVCP1 (a), EVCP2 at 75% (b) and 100% (c) SoC, and EVCP3 (d) in the 9-500 kHz frequency band during the first 50 s of measurement time together with the QP values of the amplitude of the emissions.

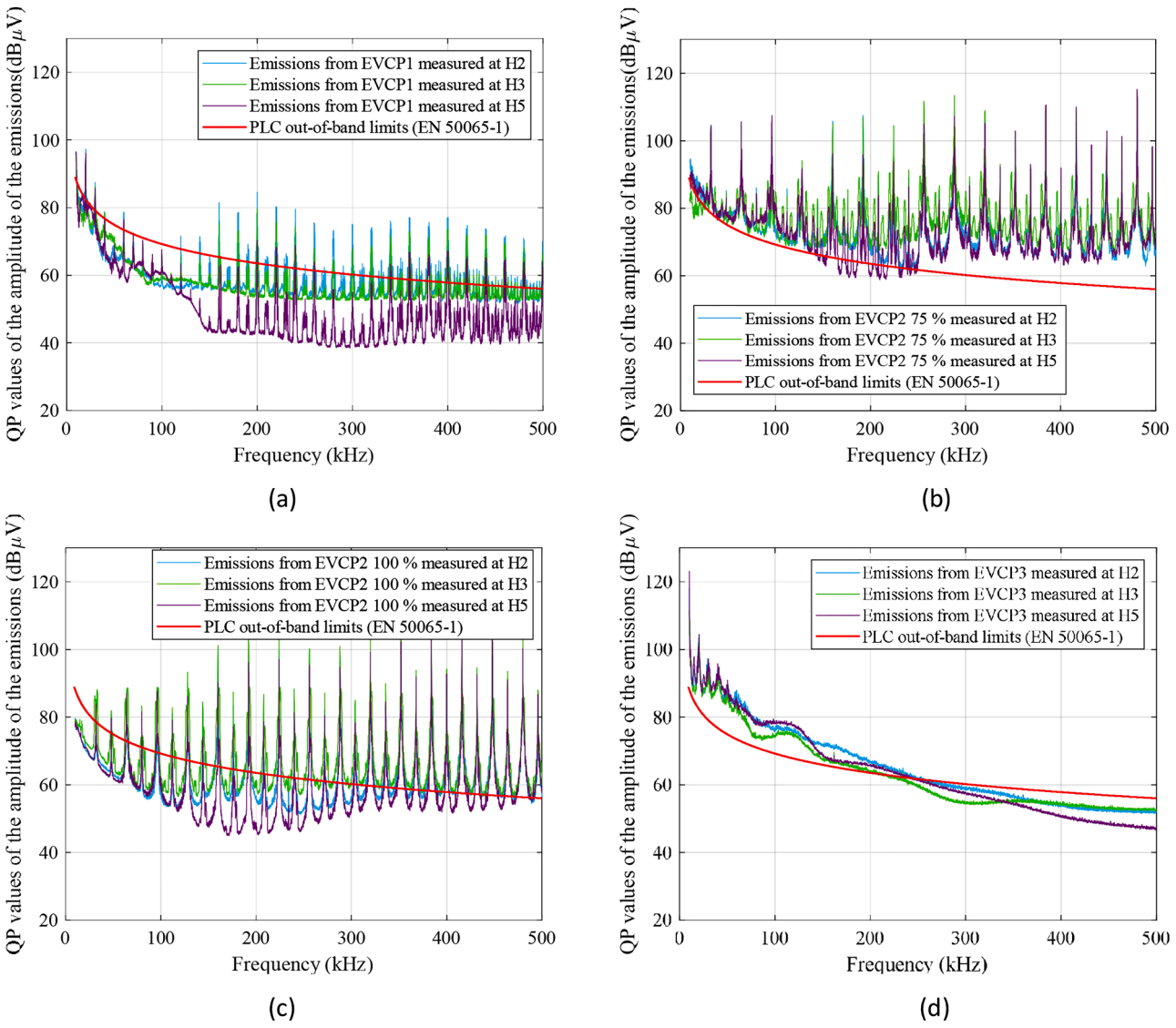

Fig. 11. Synchronized QP values of the amplitude of the emissions (dBμV) measured at H2, H3, and H5 generated by EVCP1 when EV1 is charging at H2 (a), EVCP2 at 75% and 100% SoC when EV2 is charging at H3 (b), and EVCP3 when EV3 is charging at H5 (c).

As it is stated in [46],[47], the introduction of modern energy-efficient appliances implies resonances in the grid access impedance, which may involve significant increases in the emissions at the switching frequency and its harmonics. This might be the main cause why, in spite of the attenuation suffered by the generated emissions due to the distance, the amplitudes of the disturbances are higher at an electrical point distant from the source of emissions. Hence, as it is pointed out in [23],[25],[46–48], resonances in the grid impedance are a key aspect in the amplitude of NIEs generated by electronic devices. An analysis of the influence of the grid impedance on the propagation of the disturbances is presented in [49]. Reference [7] points out that a high-impedance parallel resonance causes high-amplitude emissions at the resonance frequency, whereas a decrease in the disturbance amplitudes is observed if there is a series resonance with low impedance values.

As carried out in section V.A, in order to numerically characterize the propagation of the emissions, TSHV and PFBL values are calculated for the disturbances recorded at each location for each charging situation under test (see Table V).

The results presented in Table V lead to conclude that higher TSHVs are obtained at the POC of each house to which the EVCS under study is installed. This goes in line with the conclusions presented from Fig. 12, where, in general, a decrease in the emissions with distance was observed. The greatest difference occurs when comparing the TSHV calculated for EVCP3 at H5, 131 dBμV, and H3, 124 dBμV (difference of 7 dB). However, as concluded from Fig. 13, the distance is not the only factor affecting the amplitude of the emissions, since a resonance in the grid access impedance could imply an increase in the disturbances at that frequency. For this reason, similar or even higher TSHVs are calculated at electrical points more distant from the source of the emissions than at nearby POCs. This behavior can be observed when comparing, for example, the TSHV for EVCP1 at H3 and H5. For this EV, an identical TSHV is obtained at both locations, despite the fact that H5 is 74 meters farther away from H2 than H3. This effect arises in the four charging situations under study.

The PFBL calculated for EVCP2 at 75% SoC and EVCP3 is similar at the three POCs where the emissions are registered. In the case of EVCP2 at 75% SoC, values close to 100% (90%-100%) are obtained at the three measurement locations. The slight differences are due to the noise floor, which does not exceed the PLC out-of-band emissions limits at some frequencies when measuring the disturbances at H2 and H5. Similarly, this is the case for EVCP3, where 50% of the frequency bins (approximately up to 250 kHz) correspond to emission amplitudes above the emission limits at H2, H3, and H5. By contrast, for EVCP2 at 100% SoC,

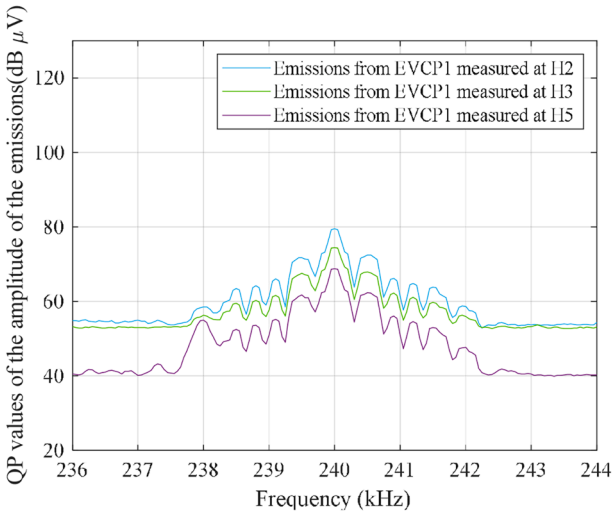

Fig. 12. Synchronized QP values of the amplitude of the emissions (dBμV) measured at H2, H3, and H5 generated by EVCP1 in the frequency range 230-250 kHz (EV1 is charging at H2).

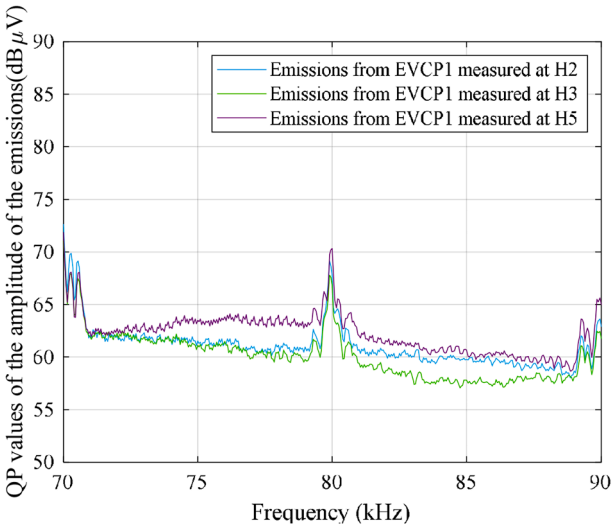

Fig. 13. Synchronized QP values of the amplitude of the emissions (dBμV) measured at H2, H3, and H5 generated by EVCP1in the frequency range 70-90 kHz (EV1 is charging at H2).

considerable differences are obtained between the PFBL calculated for the disturbances at H3 and the disturbances at H2 and H5 (differences of 23% and 35%, respectively). These variations are also mainly caused by the noise floor, since the amplitude of all the emissions exceed the limits regardless of the measurement location. Finally, for EVCP1, as the background noise is below the PLC out-of-band emissions limits in the whole frequency band at the three electrical points, it can be assumed that the variability in the PFBL can only be explained by differences in the amplitude of the narrowband emissions (see Fig. 11(a)). It should be noted that for both EVCP1 and EVCP2 at 100% SoC, the highest PFBL is obtained at the POC of the source of the emissions (at H2 for EVCP1 and at H3 for EVCP2 at 100% SoC).

6.2. *Time analysis of the propagation of the emissions*

This section aims to analyze the time variability of the emissions as they propagate through the grid. For this purpose, as carried out in section V.B.2), the FFT of the time samples corresponding to each frequency bin is calculated for the first 50-second period of the synchronized measurement of the emissions at different locations. As the modulus of the FFTs obtained for all the frequency bins fit to the expression of (7), the same procedure presented in section V.B.2) is followed and the modulus of the amplitudes of the FFT components at 50 Hz, 100 Hz, 150 Hz, and 200 Hz are normalized with respect to the modulus of the FFT component at 0 Hz for the emissions simultaneously measured at the POC of each house. Then, in order to calculate the total variability of the emissions, the sum of the amplitude of the modulus of each component is calculated according to (8). As an example, in Fig. 14, the modulus of the total variability of the disturbances generated by EVCP3 in the frequency range 9-500 kHz at H2, H3, and H5 is shown.

Fig. 14 demonstrates that the total variability of the emissions varies when propagating through the LV grid. This implies that the propagation channel introduces time-dependent variability, which, in addition, is frequency-dependent.

With the aim of analyzing the effect of the time- and frequency-dependent channel on each FFT component, the modulus of the normalized amplitude of the FFT components at 50 Hz, 100 Hz, 150 Hz, and 200 Hz of the emissions generated by EVCP3 in the frequency range 9-500 kHz when measuring the disturbances at H2, H3, and H5 are presented in Fig. 15.

Fig. 15 shows that the propagation channel has an impact on the total variability of the emissions by affecting each FFT component in a different way. This probably implies that the EVCP does not only generate emissions in the LV grid, but it also modifies the time and frequency characteristics of the propagation channel.

7. Analysis of the interaction of multiple EV charging processes

7.1. *Frequency analysis of the interaction of the emissions*

In all the results presented in the previous sections of this paper, only the individual emissions generated by a certain EVCP occurring at a specific location have been considered. However, in a real situation, these EVs are charging close to other electronic devices, which are also

Table V
TSHV and PFBL calculated for the first 50 s-period of the Synchronized measurement of the emissions at different locations.

EVCP	Measurement location	TSHV (dBμV)	PFBL (%)
Emissions from EVCP1 (EV1 charging at H2)	Emissions measured at H2	112	18
	Emissions measured at H3	110	10
	Emissions measured at H5	110	4
Emissions from EVCP2 (EV2 at 75% SoC charging at H3)	Emissions measured at H2	125	100
	Emissions measured at H3	128	97
	Emissions measured at H5	127	90
Emissions from EVCP2 (EV2 at 100% SoC charging at H3)	Emissions measured at H2	117	39
	Emissions measured at H3	122	62
	Emissions measured at H5	118	27
Emissions from EVCP3 (EV3 charging at H5)	Emissions measured at H2	128	50
	Emissions measured at H3	124	42
	Emissions measured at H5	131	48

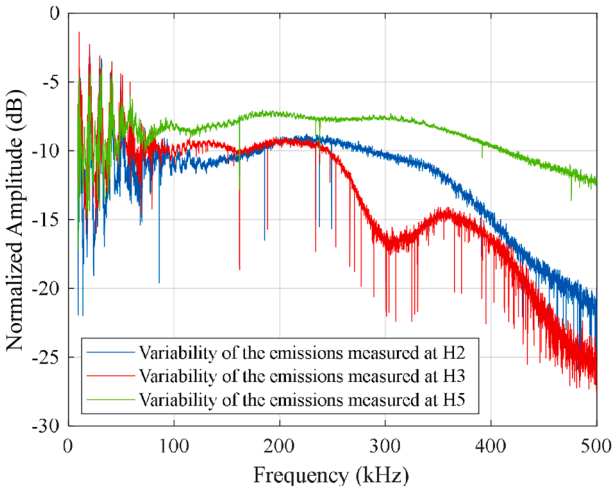

Fig. 14. Modulus of the normalized amplitude of the total variability of the emissions measured at H2, H3, and H5.

sources of disturbances. As concluded in section VI, the emissions propagate through the grid and, hence, these devices may lead to an increase in the amplitude of the emissions measured at the POC of the EV. In this section, the result of the simultaneous charging of the three EVs under study is analyzed. Fig. 16 shows, as an example, the emissions generated individually by each EVCP at H5, together with the disturbances measured when the three EVs are charging simultaneously.

As it is clearly shown, the maximum emissions measured at H5 when the three EVs are charging simultaneously can be approximated by the linear combination of the individual emissions.

First, up to 200 kHz, a spectral pattern identical to that of EVCP3 is measured, to which several narrowband emissions, generated by the charging process of EV2 at 100% SoC, are added. Second, in the frequency range 200-500 kHz, high-amplitude emissions, also corresponding to the charging process of EV2 at 100% SoC, have been registered.

However, it should also be noted that, in this frequency band, tonal emissions have been measured at specific frequencies that are not present when measuring the emissions of each EVCP individually. These narrowband emissions correspond to intermodulation products caused by the simultaneous charging of the three EVs. This goes in line with the

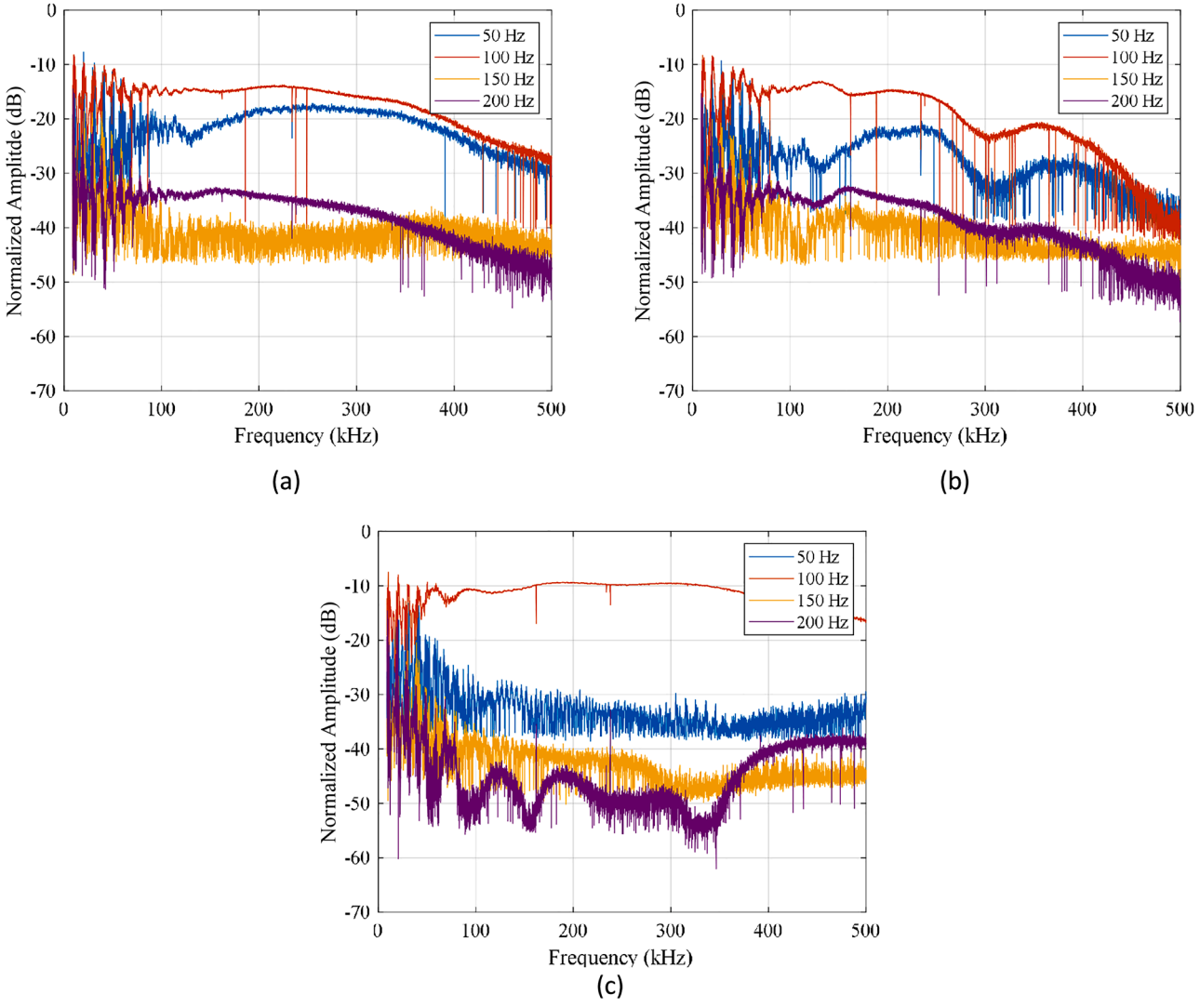

Fig. 15. Modulus of the normalized amplitude (dB) of the FFT components at 50 Hz, 100 Hz, 150 Hz, and 200 Hz of the emissions generated by EVCP3 measured at H2 (a), H3 (b), and H5 (c).

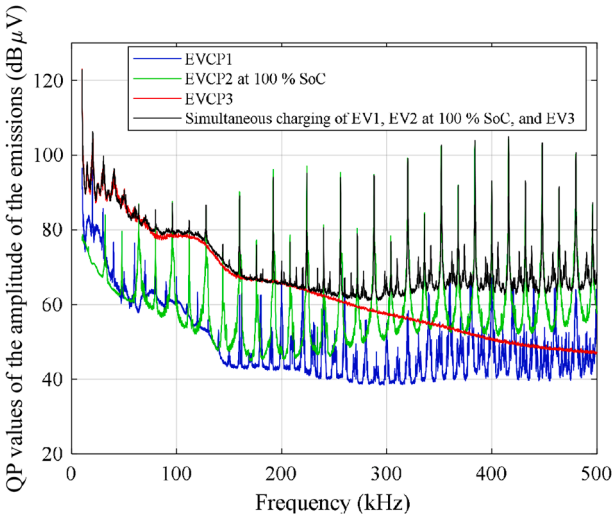

Fig. 16. QP values of the amplitude of the emissions measured at H5 when each EV is charging individually (EV1 at H2 – blue line, EV2 at 100% SoC at H3 – green line, and EV3 at H5 – red line), and when the 3 EVs are charging simultaneously – black line.

results presented in [30], where the presence of this effect is also pointed out. In order to observe this phenomenon more clearly, a zoom of the spectral pattern of the emissions due to the simultaneous charging of the three EVs in the frequency range 300-400 kHz is presented in Fig. 17, along with a linear combination of the emissions generated by the individual EVCPs, and then converted to logarithmic scale (blue line).

The previous figure shows harmonics of the switching frequency of EVCP1 (f_1 = 10 kHz) along with intermodulation products of the switching frequencies of EVCP2 at 100% SoC (f_2 = 16 kHz) and EVCP1 (f_1 = 10 kHz). Table VI compiles the harmonics and intermodulation products in the frequency range 300-400 kHz.

Finally, in order to quantify the importance of these intermodulation products in the overall amplitude of the simultaneous emissions, the TSHV and PFBL are calculated for the disturbances generated by the simultaneous EVCPs and for the linear combination of the individual emissions at H2, H3, and H5 (see Table VII).

As it is clearly shown in Table VII, similar TSHV and PFBL values are obtained for the measurement of the three simultaneous EVCPs and the approximation of linear combination of the individual EVCP emissions,

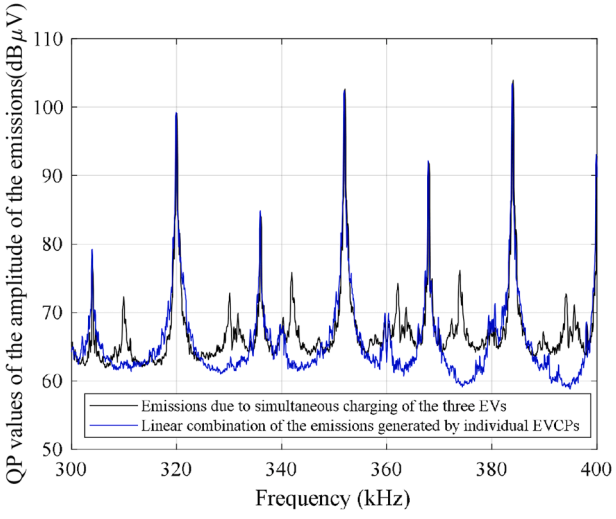

Fig. 17. Intermodulation products generated due to simultaneous charging of the three EVs in the frequency range 300-400 kHz.

Table VI
Harmonics and intermodulation products in the frequency range 300-400 kHz.

Frequency of the emission (kHz)	Type of emission		Order
310	Intermodulation	$20 \cdot f_2 - f_1$	21
320	Harmonic	$20 \cdot f_2$	20
330	Intermodulation	$20 \cdot f_2 + f_1$	21
336	Harmonic	$21 \cdot f_2$	21
342	Intermodulation	$22 \cdot f_2 - f_1$	23
352	Harmonic	$22 \cdot f_2$	22
362	Intermodulation	$22 \cdot f_2 - f_1$	23
368	Harmonic	$23 \cdot f_2$	23
374	Intermodulation	$24 \cdot f_2 - f_1$	25
384	Harmonic	$24 \cdot f_2$	24
394	Intermodulation	$24 \cdot f_2 - f_1$	25

which implies that the intermodulation products presented in Fig. 17 are not significant compared to the emissions generated by each EVCP individually.

7.2. *Time analysis of the interaction of the emissions*

As carried out in sections V.B.2) and VI.B, the time variability of the emissions generated by simultaneous EVCPs is evaluated by means of a FFT analysis. Considering that, in the previous section, we demonstrated that the emissions from simultaneous charging of the three EVs can be approximated by the linear combination of the individual EVCP emissions, we are going to analyze if this also applies to the time variability of the simultaneous emission from the three EVCPs.

In Fig. 18, the modulus of the normalized amplitude of the total variability of the simultaneous emissions from the three EVCPs and the linear combination of the emissions generated by each EVCP individually are superimposed.

In general, the variability of the emissions when the three EVs are charging simultaneously is very similar to the linear combination of the individual emissions generated by each EVCP at those frequencies where a narrowband emission is occurring. At those frequency bins where a background noise is recorded, in turn, the time variation is lower when the three EVs are charging simultaneously.

It should also be noted that the appearance of the intermodulation products reported in section IV.A due to the interaction between EVCPs is also noticeable if the total variability of the emissions is analyzed. An example of this phenomenon is presented in Fig. 19, where a zoom of the total variability is presented in the 300-400 kHz frequency band.

Fig. 19 clearly shows that, when the three EVs are charging simultaneously, the time variation of the emissions at the frequencies where intermodulation products occur (310 kHz, 330 kHz, 342 kHz, 362 kHz, 374 kHz, and 394 kHz according to Table VI) is much greater if compared to the variation of the linear combination of the emissions and may even be similar to the one presented by the narrowband emissions generated by a certain EVCP.

Finally, it is necessary to mention that approximating the emissions generated simultaneously by several EVCPs by the linear combination of the individual emissions generated by each EVCP might be only valid in case there is a predominant emission at each frequency bin. This means that, in the case that two identical EVs charge close to each other and generate identical disturbances at the same frequencies, further research

Table VII
TSHV and PFBL for the emissions generated by the simultaneous charging of the three EVs and the linear combination of the individual emissions.

	TSHV (dBμV)			PFBL (%)		
	H2	H3	H5	H2	H3	H5
Emissions from simultaneous charging of the three EVs	130	128	131	100	100	100
Linear combination of individual EVCP emissions	129	128	132	100	100	100

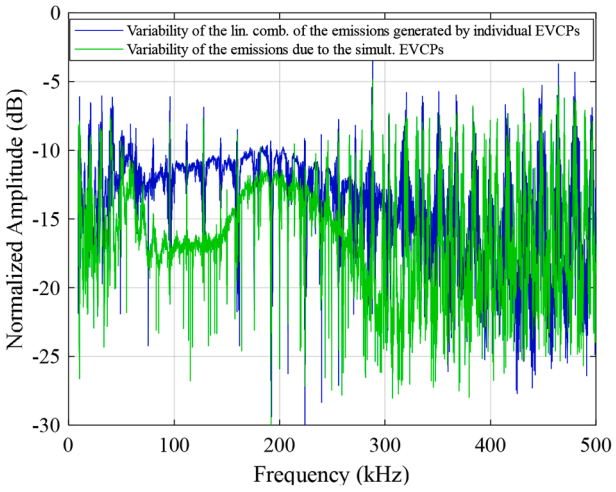

Fig. 18. Modulus of the normalized amplitude of the total variability of the simultaneous emissions from the three EVCPs and the linear combination of the emissions generated by individual EVCPs.

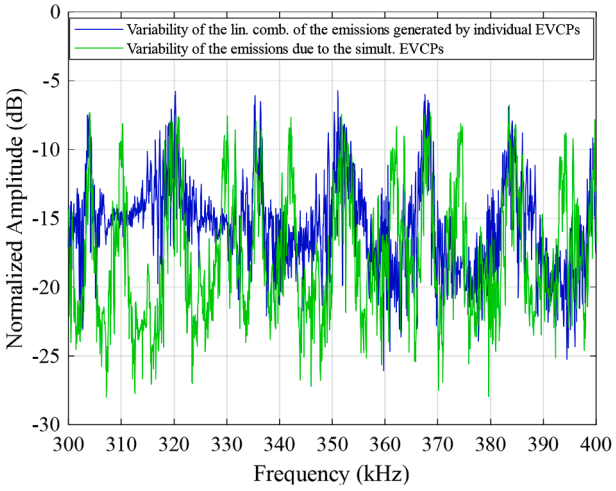

Fig. 19. Modulus of the normalized amplitude of the total variability of the simultaneous emissions from the three EVCPs and the linear combination of the emissions generated by individual EVCPs in the frequency range 300-400 kHz.

is needed.

8. Conclusions

This paper aims at characterizing, in the frequency and time domains, the emissions generated by a set of EVCPs in a controlled LV grid up to 500 kHz, as well as their capacity for propagation and interaction.

The frequency analysis shows high-amplitude emissions for the four charging situations under study. In general, the amplitude of the disturbances generated by these EVCPs exceed the limits defined in [37] for the PLC out-of-band emissions, which may involve a major negative impact on communications. The frequency characterization performed in this work demonstrates that the spectral pattern of the emissions greatly depends on the EV model, as well as on the state of charge. The calculation of the TSHV, PFBL, and CDF proposed in this paper can be useful for the complete characterization of the emissions in the frequency domain, since they allow evaluating not only the amplitude of the emissions, but also the distribution of the disturbances over the whole frequency band. Although the TSHV has already been used in the literature for the characterization of the emissions in the frequency domain, the calculation of the PFBL and CDF are novel proposals of this paper.

Moreover, a time-dependent behavior has also been observed for the four charging situations. This time analysis is performed by a novel method presented by the authors, based on FFT analysis, which allows to assess the time variations of a given emission in the LV grid by means of the complex values of five components of the FFT (50 Hz, 100 Hz, 150 Hz, 200 Hz, 250 Hz). The study points out that, although no significant time variations are registered in periods ranging from 50 s to 10 minutes (maximum difference in the TSHV of 3 dB between periods of 50 s within the measuring time), variations occur within the mains cycle. These short-term variations, together with the high-amplitude disturbances, might have negative effects on the estimation and equalization processes defined by PLC technologies. As the equalization is based on previous estimations of the propagation channel, fast variations in the emissions could considerably condition the proper performance of PLC. In addition, long-term variations due to different states of charge are also expected. In order to prove this, long-term measurements need to be performed.

The results also lead to conclude that these disturbances propagate through the LV grid for several tens of meters, which can be typical distances between consumers in real grids in urban or semi-urban scenarios. In general, the spectral features of the emissions are maintained when measuring at electrical points distant from the source, but their amplitudes are attenuated with distance. An example of this is reported for EVCP2 at 100% SoC. While the TSHV at the POC where the EVCS is installed (H3) is 122 dBμV, this parameter is reduced 5 dB when measuring the emissions generated by this EVCP at H2 and 4 dB when the measurement is performed at H5. However, in some cases, emissions with higher amplitudes are measured at locations different from the POC of the EV at specific frequencies, which may be due to resonances in the resultant grid impedance. It should also be noted that different time variations in the amplitude of the NIEs have been observed depending on the measurement location of the emissions, due to the time-dependent behavior of the propagation channel.

Finally, the effect of the simultaneous charging of the three EVs on the NIEs has been analyzed, concluding that, in general, the disturbances when multiple EVs are charging simultaneously are well aligned with the linear combination of the individual emissions in case there is a predominant emission at each frequency bin.

Although the emissions generated by an EVCP depend on the specific measurement scenario, the results presented in this paper demonstrate that this is a complex phenomenon that requires further consideration. Future studies should consider different measurement scenarios, in which the emissions generated by a wide range of EV models are evaluated, taking into consideration different chargers (AC/DC), charging currents, and SoCs. For this purpose, the methodology proposed in this paper could be applied, which allows the characterization of any conducted emission in the LV grid in the frequency and time domains, as well as their propagation and interaction through the network. Besides, the evaluation of the potential influence of these disturbances on NB-PLC is also a matter to be analyzed. In this way, robust data coding algorithms and modulations adapted to the amplitude, spectral shape, and time-dependent behavior of the emissions could be designed, in order to achieve a better performance of NB-PLC systems.

CRediT authorship contribution statement

Jon González-Ramos: Conceptualization, Data curation, Software, Writing – original draft. **Alexander Gallarreta:** Methodology, Validation. **Igor Fernández:** Methodology, Software. **Itziar Angulo:** Conceptualization, Supervision, Writing – original draft, Writing – review & editing. **David de la Vega:** Funding acquisition, Project administration. **Amaia Arrinda:** Supervision.

Declaration of competing interest

The authors declare that they have no known competing financial interests or personal relationships that could have appeared to influence the work reported in this paper.

Data availability

Data will be made available on request.

Acknowledgments

This work was supported in part by the Basque Government under Grants IT1436–22, PRE_2022_2_0074 and PRE_2022_2_0244, and in part by the Spanish Government under Grant PID2021–124706OB-I00, funded by MCIN/AEI/10.13039/501100011033 and ERDF A way of making Europe.

The authors would like to thank Daniela Istrate (LNE) and Paul Wright (NPL) for their collaboration in this work in the context of JRP SupraEMI project, and Électricite de France (EDF) for the availability and the collaboration of authorized staff for carrying out the field trials.

References

[1] M.A. van den Berg, I. Lampropoulos, T.A. AlSkaif, Impact of electric vehicles charging demand on distribution transformers in an office area and determination of flexibility potential, Sustainable Energy, Grids and Networks 26 (2021) 100452, https://doi.org/10.1016/j.segan.2021.100452.

[2] J.A. Sanguesa, V. Torres-Sanz, P. Garrido, F.J. Martinez, J.M. Marquez-Barja, A Review on Electric Vehicles: Technologies and Challenges, Smart Cities 4 (1) (2021) 372–404, https://doi.org/10.3390/smartcities4010022.

[3] L. Wang, Z. Qin, T. Slangen, P. Bauer, T. van Wijk, Grid Impact of Electric Vehicle Fast Charging Stations: Trends, Standards, Issues and Mitigation Measures - An Overview, IEEE Open. J. Power. Electron. 2 (2021) 56–74, https://doi.org/10.1109/OJPEL.2021.3054601.

[4] M. Wasowski, et al., Sources of Non-Intentional Supraharmonics in LV Network and Its Impact on OSGP PLC Communication – Experimental Study, IEEE Transactions on Power Delivery 37 (6) (2022) 5244–5254, https://doi.org/10.1109/TPWRD.2022.3175090.

[5] S.K. Ronnberg, M.H.J. Bollen, M. Wahlberg, Interaction Between Narrowband Power-Line Communication and End-User Equipment, IEEE Transactions on Power Delivery 26 (3) (2011) 2034–2039, https://doi.org/10.1109/TPWRD.2011.2130543.

[6] A. Llano, D. De La Vega, I. Angulo, L. Marron, Impact of Channel Disturbances on Current Narrowband Power Line Communications and Lessons to Be Learnt for the Future Technologies, IEEe Access. 7 (2019) 83797–83811, https://doi.org/10.1109/ACCESS.2019.2924806.

[7] B. Grasel, J. Baptista, M. Tragner, Supraharmonic and Harmonic Emissions of a Bi-Directional V2G Electric Vehicle Charging Station and Their Impact to the Grid Impedance, Energies. (Basel) 15 (8) (2022), https://doi.org/10.3390/en15082920.

[8] J. Sutaria, S.K. Rönnberg, Propagation of Supraharmonics in a Data Center With Different Operating Modes of UPS, IEEE Access. 11 (2023) 36823–36833, https://doi.org/10.1109/ACCESS.2023.3266092.

[9] Ł. Michalec, P. Kostyła, Z. Leonowicz, Supraharmonic Pollution Emitted by Nonlinear Loads in Power Networks—Ongoing Worldwide Research and Upcoming Challenges, Energies. (Basel) 16 (1) (2023), https://doi.org/10.3390/en16010273.

[10] G. Foskolos, Measurement-Based Current-Harmonics Modeling of Aggregated Electric-Vehicle Loads Using Power-Exponential Functions, World Elect. Veh. J. 11 (3) (2020), https://doi.org/10.3390/wevj11030051.

[11] A. Supponen, A. Rautiainen, J. Markkula, A. Mäkinen, P. Järventausta, S. Repo, Power quality in distribution networks with electric vehicle charging - a research methodology based on field tests and real data, in: 2016 Eleventh International Conference on Ecological Vehicles and Renewable Energies (EVER), 2016, pp. 1–11, https://doi.org/10.1109/EVER.2016.7476376.

[12] N. Melo, F. Mira, A. de Almeida, J. Delgado, Integration of PEV in Portuguese distribution grid: Analysis of harmonic current emissions in charging points, in: 11th International Conference on Electrical Power Quality and Utilisation, 2011, pp. 1–6, https://doi.org/10.1109/EPQU.2011.6128893.

[13] J. Meyer, S. Mueller, S. Ungethuem, X. Xiao, A. Collin, S. Djokic, Harmonic and supraharmonic emission of on-board electric vehicle chargers, in: 2016 IEEE PES Transmission & Distribution Conference and Exposition-Latin America (PES T&D-LA), 2016, pp. 1–7, https://doi.org/10.1109/TDC-LA.2016.7805641.

[14] S. Lodetti, J. Bruna, J.F. Sanz, J.J. Melero, Characterization of the Emission of an Electric Bus Inductive Charging in the 2 kHz to 150 kHz Range, in: 2019 AEIT International Conference of Electrical and Electronic Technologies for Automotive (AEIT AUTOMOTIVE), 2019, pp. 1–6, https://doi.org/10.23919/EETA.2019.8804604.

[15] T.M.H. Slangen, T. van Wijk, V. Ćuk, J.F.G. Cobben, The Harmonic and Supraharmonic Emission of Battery Electric Vehicles in The Netherlands, in: 2020 International Conference on Smart Energy Systems and Technologies (SEST), 2020, pp. 1–6, https://doi.org/10.1109/SEST48500.2020.9203533.

[16] S. Schöttke, J. Meyer, P. Schegner, S. Bachmann, Emission in the frequency range of 2 kHz to 150 kHz caused by electrical vehicle charging, in: 2014 International Symposium on Electromagnetic Compatibility, 2014, pp. 620–625, https://doi.org/10.1109/EMCEurope.2014.6930980.

[17] D. Darmawardana, J. David, S. Perera, D. Robinson, J. Meyer, U. Jayatunga, Analysis of High Frequency (Supraharmonics) Emissions Caused by Electric Vehicle Charging, in: 2020 19th International Conference on Harmonics and Quality of Power (ICHQP), 2020, pp. 1–6, https://doi.org/10.1109/ICHQP46026.2020.9177932.

[18] J. González-ramos, I. Fernández, I. Angulo, A. Gallarreta, D.D. La Vega, A. Arrinda, Empirical characterization of the conducted disturbances generated by the electric vehicles during the charging process, in: CIRED Porto Workshop2022: E-mobility and power distribution systems, 2022, pp. 319–323, https://doi.org/10.1049/icp.2022.0719.

[19] A. Novitskiy, S. Schlegel, D. Westermann, Analysis of supraharmonic propagation in a MV electrical network, in: 2018 19th International Scientific Conference on Electric Power Engineering (EPE), 2018, pp. 1–6, https://doi.org/10.1109/EPE.2018.8396041.

[20] Á. Espín-Delgado, T. Busatto, V. Ravindran, S.K. Rönnberg, J. Meyer, Evaluation of Supraharmonic Propagation in LV Networks Based on the Impedance Changes Created by Household Devices, in: 2020 IEEE PES Innovative Smart Grid Technologies Europe (ISGT-Europe), 2020, pp. 754–758, https://doi.org/10.1109/ISGT-Europe47291.2020.9248928.

[21] A. Novitskiy, S. Schlegel, D. Westermann, Measurements and Analysis of Supraharmonic Influences in a MV/LV Network Containing Renewable Energy Sources, in: 2019 Electric Power Quality and Supply Reliability Conference (PQ) & 2019 Symposium on Electrical Engineering and Mechatronics (SEEM), 2019, pp. 1–6, https://doi.org/10.1109/PQ.2019.8818260.

[22] S. Rönnberg and M. Bollen, "Propagation of Supraharmonics in the Low Voltage Grid", Report 2017:461, Elektra," 2017.

[23] S. Cassano, F. Silvestro, E.D. Jaeger, C. Leroi, Modeling of harmonic propagation of fast DC EV charging station in a Low Voltage network, in: 2019 IEEE Milan PowerTech, 2019, pp. 1–6, https://doi.org/10.1109/PTC.2019.8810969.

[24] S. Rönnberg, A. Larsson, M. Bollen, J.L. Schanen, A simple model for interaction between equipment at a frequency of some tens of kHz, in: 21st International Conference on Electricity Distribution (CIRED), 2011.

[25] S. K. Ronnberg, M. H. J. Bollen, A. Larsson, and M. Lundmark, "An overview of the origin and propagation of Supraharmonics (2-150 kHz)," 2014.

[26] J. Sutaria, S. Rönnberg, Á. Espín-Delgado, Analysis of supraharmonics in a three-phase frame, Electric Power Systems Research 203 (2022) 107668, https://doi.org/10.1016/j.epsr.2021.107668.

[27] T. Slangen, V. Ćuk, S. Cobben, Summation of supraharmonic currents (2–150 kHz) from EV fast charging stations, Electric Power Systems Research 220 (2023) 109371, https://doi.org/10.1016/j.epsr.2023.109371.

[28] T. Busatto, F. Abid, A. Larsson, M.H.J. Bollen, G. Singh, Interaction between grid-connected PV systems and LED lamps: Directions for further research on harmonics and supraharmonics, in: 2016 17th International Conference on Harmonics and Quality of Power (ICHQP), 2016, pp. 193–197, https://doi.org/10.1109/ICHQP.2016.7783479.

[29] T. Streubel, C. Kattmann, A. Eisenmann, K. Rudion, Characterization of Supraharmonic Emission from Three Different Electric Vehicle Charging Infrastructures in Time and Frequency Domain, Energies. (Basel) 15 (2) (2022), https://doi.org/10.3390/en15020394.

[30] T. Slangen, T. van Wijk, V. Ćuk, S. Cobben, The Propagation and Interaction of Supraharmonics from Electric Vehicle Chargers in a Low-Voltage Grid, Energies. (Basel) 13 (15) (2020), https://doi.org/10.3390/en13153865.

[31] I. Fernandez, et al., Characterization of non-intentional emissions from distributed energy resources up to 500 kHz: A case study in Spain, Int. J. Elect. Pow. Energ. Syst. 105 (2019) 549–563, https://doi.org/10.1016/j.ijepes.2018.08.048.

[32] J. Sutaria, Á. Espín-Delgado, S. Rönnberg, Supraharmonics within a Datacenter-Emission and Propagation, in: 2022 20th International Conference on Harmonics & Quality of Power (ICHQP), 2022, pp. 1–6, https://doi.org/10.1109/ICHQP53011.2022.9808561.

[33] "Specification for Radio Disturbance and Immunity Measuring Apparatus and Methods—Part 1-1: Radio Disturbance and Immunity Measuring Apparatus—Measuring Apparatus, document CISPR 16-1-1:2019," 2019.

[34] "Technical Specification of the NSQC442G Electric Vehicle Charging Station".

[35] "Technical Specification of the Witty XEV100 Electric Vehicle Charging Station".

[36] I. Fernández, M. Alberro, J. Montalbán, A. Arrinda, I. Angulo, D. de la Vega, A new voltage probe with improved performance at the 10 kHz–500 kHz frequency range for field measurements in LV networks, Measurement 145 (2019) 519–524, https://doi.org/10.1016/j.measurement.2019.05.106.

[37] "CENELEC EN 50065-1. Signaling on low voltage installations in the frequency range 3 kHz to 148.5 kHz – Part 1: general requirements, frequency bands and electromagnetic disturbances," 2011.

[38] G.F. Bartak, A. Abart, EMI of emissions in the frequency range 2 kHz–150 kHz, in: 22nd International Conference and Exhibition on Electricity Distribution (CIRED2013), 2013, pp. 1–4, https://doi.org/10.1049/cp.2013.1151.

[39] G. López, J.I. Moreno, E. Sánchez, C. Martínez, F. Martín, Noise Sources, Effects and Countermeasures in Narrowband Power-Line Communications Networks: A

Practical Approach, Energies. (Basel) 10 (8) (2017), https://doi.org/10.3390/en10081238.
[40] A. Mariscotti, Harmonic and Supraharmonic Emissions of Plug-In Electric Vehicle Chargers, Smart Cities 5 (2) (2022) 496–521, https://doi.org/10.3390/smartcities5020027.
[41] A. Prudenzi, A. Fioravanti, A. Silvestri, F. Ciancetta, E. Fiorucci, S. Mari, Overview of the Propagation of Supraharmonics in Power Systems, in: 2022 AEIT International Annual Conference (AEIT), 2022, pp. 1–6, https://doi.org/10.23919/AEIT56783.2022.9951834.
[42] A. Grevener, J. Meyer, S. Rönnberg, M. Bollen, J.M.A. Myrzik, Survey of supraharmonic emission of household appliances, CIRED Open Access Proc. J. 2017 (Oct. 2017) 870–874, https://doi.org/10.1049/oap-cired.2017.0458.
[43] "PRIME Alliance, 'PRIME v1.4 White Paper', PRIME Alliance," Brussels, 2014. Accessed: Sep. 18, 2023. [Online]. Available: https://www.prime-alliance.org/media/2020/04/whitePaperPrimeV1p4_final.pdf.
[44] S.H. Hwang, Y. Chen, H. Zhang, K.Y. Lee, D.H. Kim, Reconfigurable Hybrid Resonant Topology for Constant Current/Voltage Wireless Power Transfer of Electric Vehicles, Electronics. (Basel) 9 (8) (2020), https://doi.org/10.3390/electronics9081323.
[45] J.D. McK, Ed. Watson, Digital Signal Processing: principles, devices and applications. Control, Robotics and Sensors, Institution of Engineering and Technology, 1990 [Online]. Available: https://digital-library.theiet.org/content/books/ce/pbce042e.
[46] M. Lundmark, "The Zone Concept: Design of Low Voltage Installations Considering the Spread of High Frequency Harmonics," Lulea, 2010.
[47] S. Rönnberg, "Emissions and Interaction from Domestic Installations in the Low Voltage Electricity Network, up to 150 kHz," Lulea, 2013.
[48] S.K. Rönnberg, et al., On waveform distortion in the frequency range of 2kHz–150kHz—Review and research challenges, Electric Power Systems Research 150 (2017) 1–10, https://doi.org/10.1016/j.epsr.2017.04.032.
[49] Á. Espín-Delgado, S. Rönnberg, Modeling and Analysis of Supraharmonic Propagation for Stochastic Studies, IEEE Transactions on Power Delivery 37 (6) (2022) 4899–4910, https://doi.org/10.1109/TPWRD.2022.3162712.